EARTHQUAKE ENGINEERING AND STRUCTURAL DYNAMICS, VOL. 25, 727–742 (1996)

FIBRE BEAM–COLUMN MODEL FOR NON-LINEAR ANALYSIS OF R/C FRAMES: PART II. APPLICATIONS

ENRICO SPACONE*
Department of Civil, Environmental, and Architectural Engineering, University of Colorado, Boulder, CO 80309-0428, U.S.A.

AND

FILIP C. FILIPPOU† AND FABIO F. TAUCER‡
Department of Civil Engineering, University of California, Berkeley, CA 94720-1710, US.A.

SUMMARY

A companion paper presents the formulation of a fibre beam-column element for the non-linear static and dynamic analysis of R/C frames. This paper illustrates the application of the proposed element in the simulation of the hysteretic behaviour of several R/C beam and column specimens. The specimens are subjected to uniaxial and biaxial loading histories with varying axial load. The proposed element shows computationally stable and robust numerical behaviour, while being able to describe very well the hysteretic behaviour of the reinforced concrete members under the imposed complex loading histories.

KEY WORDS: beam–column; biaxial response; hysteretic behaviour; reinforced concrete

INTRODUCTION

The objective of this paper is to illustrate the ability of the element proposed in the companion paper by Spacone *et al.*[1] in simulating the hysteretic behaviour of reinforced concrete members under complex load histories. The selected specimens are of gradually increasing complexity starting from a reinforced concrete section, followed by a cantilever beam with no axial force and concluding with a cantilever column under constant as well as varying axial force. While the section and cantilever beam are subjected to a cyclic uniaxial curvature and a cyclic uniaxial tip displacement, respectively, the cantilever column is investigated under three different load histories: a uniaxial cyclic tip displacement in one principal direction; a cyclic tip displacement in a direction that does not coincide with a principal axis and, thus, induces biaxial response; and, a cyclic tip displacement in a cloverleaf pattern with simultaneously varying axial force.

The material parameters for modelling the specimens are obtained from available experimental information through coupon or concrete cylinder tests. The hysteretic behaviour of concrete and reinforcing steel is simulated with the material models described in Spacone *et al.*[1] The tensile strength of concrete is neglected in the simulations and tension stiffening effects are neglected, since the objective of the study is the hysteretic response under large inelastic deformations, when this effect does not play a significant role on the response.

The simulations of the load–displacement response of the specimens are performed with program FEDEAS,[2] a structural element library that is integrated with the general purpose finite element program FEAP developed by Professor Taylor at the University of California, Berkeley and documented in Zienkiewicz and Taylor.[3,4] The structural element library is responsible for the modelling of the elements, while

*Assistant Professor
†Associate Professor
‡Research Assistant. Presently with T. Y. Lin International, San Francisco, CA, U.S.A.

CCC 0098-8847/96/070727-16

Received 10 August 1995
Revised 18 January 1996

the core program handles the input, output and storage of structural data and controls the nonlinear solution strategy for static and dynamic excitations.

MOMENT–CURVATURE OF RC SECTION

The fibre section model lies at the heart of the fibre beam-column element and controls its hysteretic behaviour through the non-linear material models of the individual fibres. It is a very useful model in its own right for the study of the hysteretic behaviour of RC sections and plastic hinge regions. Moreover, the performance of the fibre beam-column element largely depends on the interaction of the control sections of the element and, thus, a thorough understanding of the section behaviour is also important from an analytical standpoint. Some of the physical and numerical issues that can be addressed in a study of hysteretic section behaviour are: (a) the effect of axial load on the hysteretic moment–curvature relation under uniaxial and biaxial moments; (b) the effect of section discretization, i.e. number and position of fibres, on the accuracy of the results; (c) the effect of material models on the accuracy of the results, noting that the numerical effort of a fibre material model will have considerable impact on the computational cost and, consequently, practical feasibility of the non-linear dynamic analysis of the model of a multistorey frame structure that consists of fibre beam-column elements. These issues are beyond the scope of this paper and are addressed in some detail by Spacone.[5] Here the hysteretic behaviour of a reinforced concrete section and a parametric study of the effect of axial force on the flexural response are briefly discussed. These studies are conducted with the hinge element in FEDEAS, which consists of a single section that is subdivided into fibres. The element has no physical length, so that it can represent the hysteretic moment–rotation relation at hinges and connections.

The RC section selected for the correlation study was previously studied by Kent[6] in an integrated experimental and analytical study in connection with the hysteretic behaviour of RC cantilever beams. The measured material properties for the cantilever beam, as reported by Kent,[6] are summarized in Tables I and II, where E_c denotes the initial concrete modulus, f_c' the concrete compressive strength, ε_0 the concrete strain at maximum stress, ε_u the ultimate concrete strain, E_s the initial steel modulus and f_y the yield strength of reinforcing steel. Only the unconfined concrete properties were measured by Kent.[6] The confined concrete properties in Table I were derived with the model of Kent–Park, as later modified by Scott *et al.*[7] The cantilever beam was loaded with a transverse concentrated load at the free end and the hysteretic behaviour was measured near the built-in end of the beam. The measured response by Kent[6] and the analytical results with his fibre section model are shown in Figure 1.

Figure 2 shows the hysteretic moment–curvature relation with the hinge element in program FEDEAS. The insets of Figure 2 show the geometry of the cross-section and its subdivision into the unconfined cover

Table I. Material properties of concrete (1 ksi = 6·894 MPa)

Concrete properties				
Concrete type	E_c (ksi)	f_c' (ksi)	ε_0	ε_u
Unconfined	3605	−6·95	−0·0027	−0·00292
Confined	3605	−6·95	−0·0027	−0·03810

Table II. Material properties of reinforcing steel (1 ksi = 6·894 MPa)

Steel properties			
Steel type	E_s (ksi)	f_y (ksi)	Strain hard. ratio
Steel	29,000	48·4	0·0042

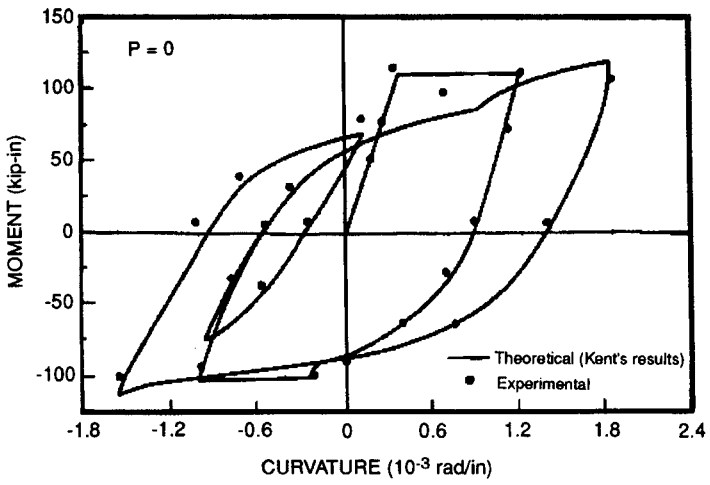

Figure 1. Moment–curvature relation from Kent's experiment and Kaba–Mahin analysis in Reference 13 (1 in = 2·54 cm, 1 kip = 4·448 kN)

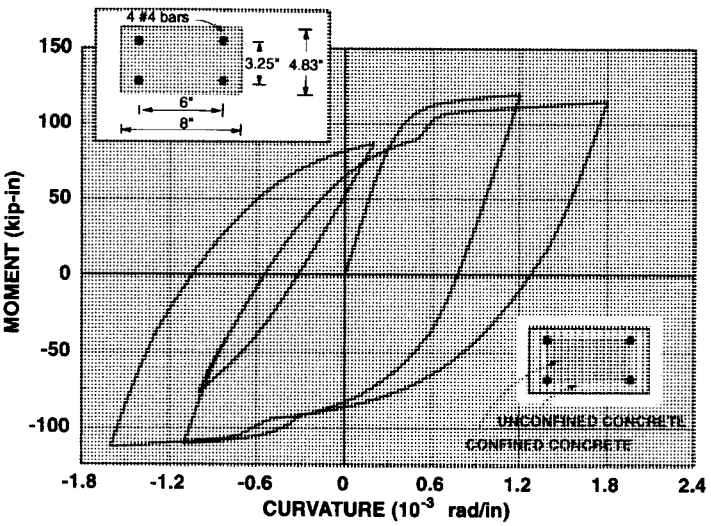

Figure 2. Analytical moment–curvature relation for Kent's specimen (1 in = 2·54 cm, 1 kip = 4·448 kN)

concrete and the confined core concrete. Since the section is only subjected to uniaxial bending, it is subdivided into layers, rather than fibres, with 12 layers in the core and 3 layers in the top and bottom cover. The analytical results in Figure 2 are in excellent agreement with the observed experimental behaviour. This agreement is slightly superior to that of the analytical results of Kent. The only slight discrepancy occurs at the transition between the initial elastic branch and the post-yield plateau: the model exhibits a rounded, gradual transition, as opposed to the sharp transition of the experimental results. This is a characteristic of the Menegotto–Pinto steel model used in this study. It is worth noting that the numerical scheme used in the state determination of the section is path-independent, so that the accuracy of the results in Figure 2 is not affected by the curvature step size, as the parametric studies in Reference 8 demonstrate. The smooth response in Figure 2, however, requires a small step size.

Figure 3 shows the results of a parametric study on the effect of axial force on the flexural response of the cross-section of Kent's specimen. The axial force levels range from a tensile axial force of 5 per cent $f'_c A_c$ to

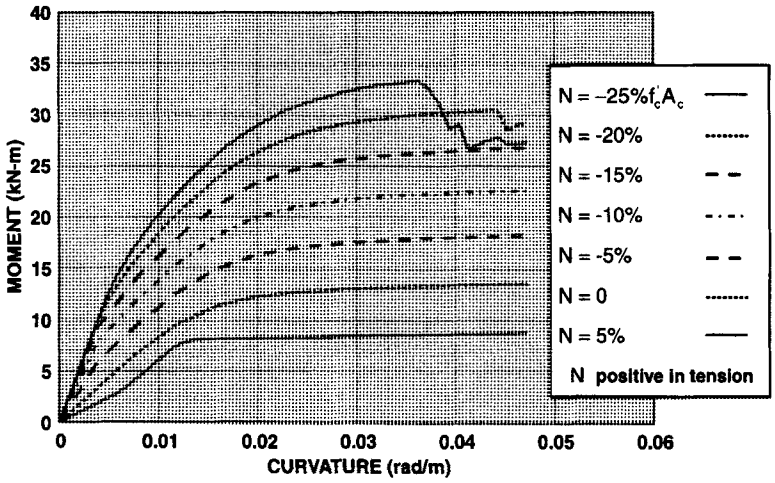

Figure 3. Effect of axial force on flexural response of RC section

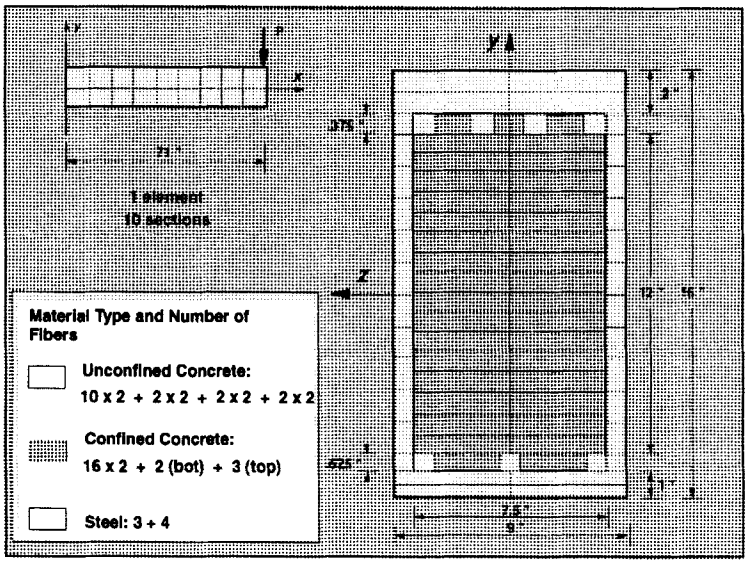

Figure 4. Structure discretization for beam R1 (1 in = 2·54 cm)

a compressive axial force of 25 per cent $f_c'A_c$ in increments of 5 per cent $f_c'A_c$. Since the axial force of 25 per cent $f_c'A_c$ is less than the balance load, the increase in axial force causes an increase in the initial section stiffness and the ultimate strength of the section. At the same time the increase in axial force leads to a reduction in curvature ductility. The characteristic stepped drop in bending resistance, as the outermost section layers reach one by one the ultimate (crushing) strain, is evident in the moment–curvature relation under an axial force of 20 per cent $f_c'A_c$ and 25 per cent $f_c'A_c$ in Figure 3.

UNIAXIAL BENDING OF CANTILEVER BEAM

An extensive series of tests on rectangular and T-shaped reinforced concrete beams was conducted by Ma *et al.*[9] The following correlation studies refer to the rectangular beam R1. The geometry of the specimen and the discretization of the cross-section are shown in Figure 4. The relevant geometric data are summarized in

Table III, while Tables IV and V contain the material parameters for the concrete and reinforcing steel models, respectively. These parameters are derived from available experimental information from coupon and concrete cylinder tests. In simulating the behaviour of confined concrete the model by Scott *et al.*[7] was used. In this model the degree of confinement depends on the volumetric ratio of transverse reinforcement relative to the confined concrete core ρ_s which for beam R1 was estimated at 0·60 per cent.

The numerical simulation of the hysteretic behaviour of the cantilever was conducted by imposing the measured displacement at the tip of the cantilever model. This measured displacement arises from flexural deformations, shear deformations, bond-slip between concrete and reinforcing steel and the rotation at the built-in section due to reinforcing bar pull-out from the column stub. Since the analytical model presently only accounts for flexural deformations, the analytical results in Figure 5 deviate from the experimental data in Figure 6. The discrepancy is small before yielding at the built-in section of the cantilever takes place, but increases in the post-yield cycles and is particularly noticeable during reloading in the 'pinching' of the experimental hysteretic loop due to shear and bond-slip.

The analytical and experimental moment–curvature relation near the built-in section of the cantilever are shown in Figures 7 and 8, respectively. The agreement is much better in this case, since the other sources of inelastic deformation do not affect the hysteretic section response that much.

UNIAXIAL AND BIAXIAL BENDING UNDER CONSTANT AXIAL COMPRESSION

A series of columns were tested under different load histories of uniaxial and biaxial bending under, both, constant and variable axial force by Low and Moehle.[10] The columns had rectangular cross-section, were fixed at the base and were subjected to a concentrated axial load and imposed lateral displacements at the free end, as shown in Figure 9. The amount of transverse reinforcement changed at specimen mid-height. The lower half of the column had a volumetric ratio of transverse reinforcement relative to the confined concrete

Table III. Beam R1 discretization

Cantilever beam R1				
Number of beam-column elements: 1				
Length of element = 71 in			Number of Sections = 10	
	Number of fibres			
Section type	Unconfined concrete	Confined concrete	Steel	Total
I	16 × 2	20 × 2	7	79

Table IV. Concrete material properties (1 ksi = 6·894 MPa)

Concrete properties				
Concrete type	E_c (ksi)	f'_c (ksi)	ε_0	ε_u
Unconfined	3980	−5·07	−0·00200	−0·003
Confined	3980	−5·43	−0·00214	−0·069

Table V. Steel material properties (1 ksi = 6·894 MPa)

Steel properties			
Steel type	E_s (ksi)	f_y (ksi)	Strain hard. ratio
Steel type 1	29,000	66·5	0·0085

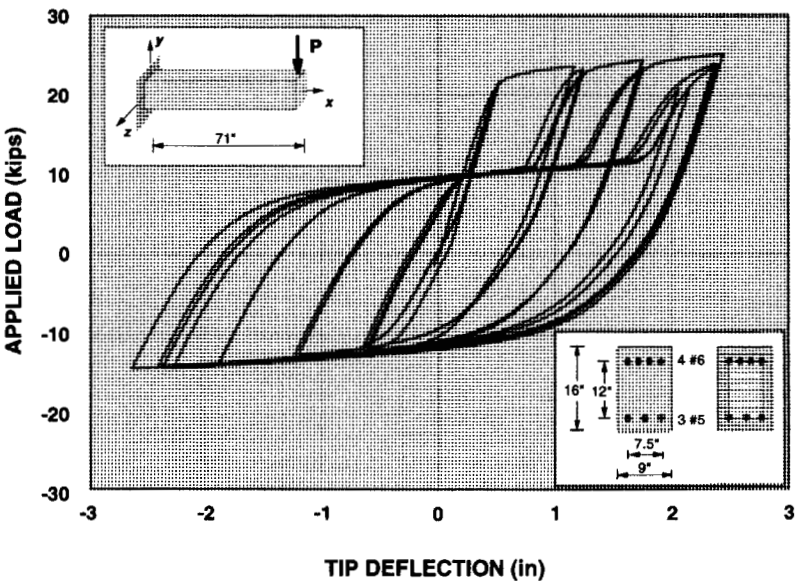

Figure 5. Analytical load–tip displacement relation for beam R1 (1 in = 2·54 cm, 1 kip = 4·448 kN)

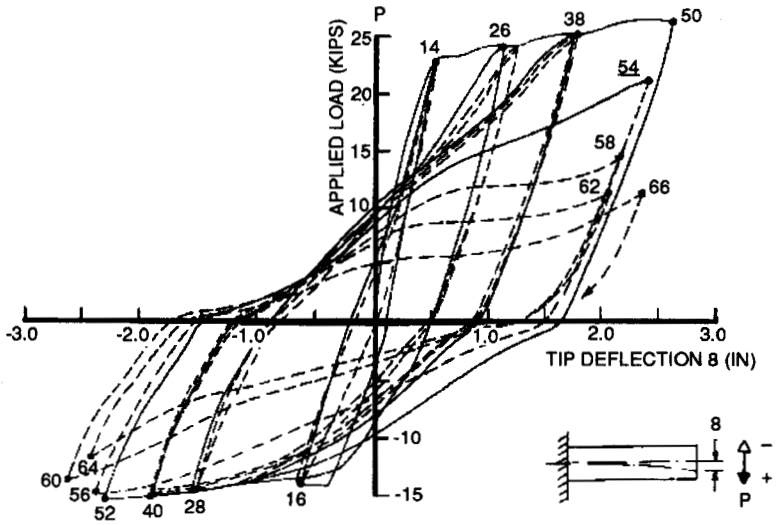

Figure 6. Measured tip load–displacement relation for beam R1[9] (1 in = 2·54 cm, 1 kip = 4·448 kN)

core ρ_s equal to 2 per cent. This corresponds to section type I. The upper half of the column had a volumetric ratio of transverse reinforcement relative to the confined concrete core ρ_s equal to 1·3 per cent and corresponds to section type II (Table VI). The material parameters of the specimens, as derived from coupon and concrete cylinder tests, are summarized in Table VII.

The correlation studies in this section refer to Specimens #1 and #2, which were subjected to a constant axial force. Specimen #1 was subjected to a cyclic uniaxial lateral force inducing flexure about the strong column axis and an axial compression of 44·5 kN that corresponds approximately to 5 per cent $f'_c A_c$. The model consists of a single beam-column element that contains two types of section in accordance with the amount of transverse reinforcement in the specimen. A very fine subdivision is used for each cross-section and four Gauss–Lobatto integration points are used for monitoring the inelastic behaviour of the entire column.[8] The hysteretic behaviour of confined concrete is described by the model of Scott *et al.*[7]

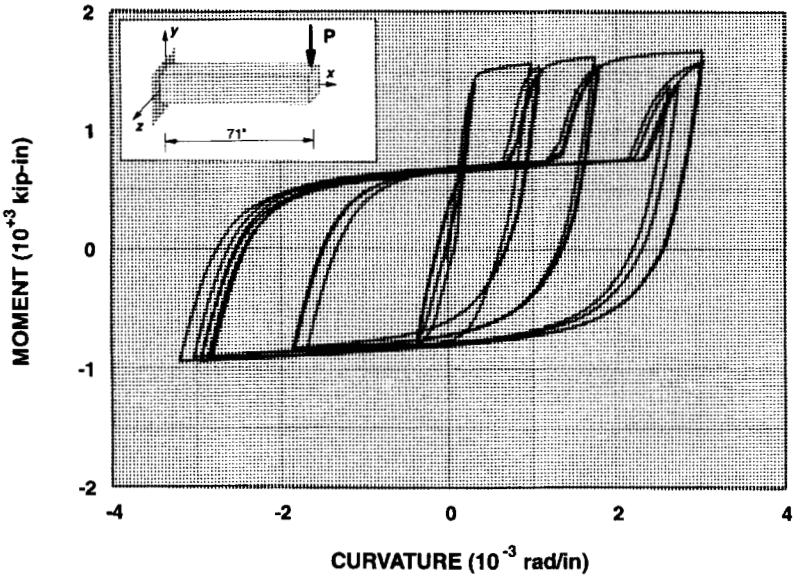

Figure 7. Analytical moment–curvature relation near built-in section of Beam R1 (1 in = 2·54 cm, 1 kip = 4·448 kN)

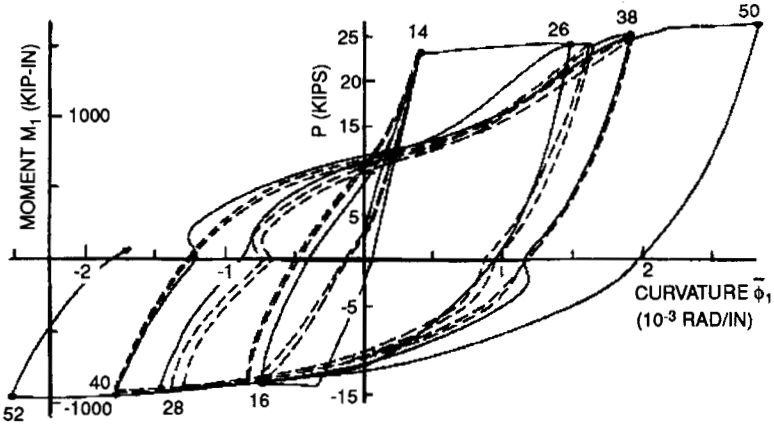

Figure 8. Measured moment–curvature relation near built-in section of Beam R1[9] (1 in = 2·54 cm, 1 kip = 4·448 kN)

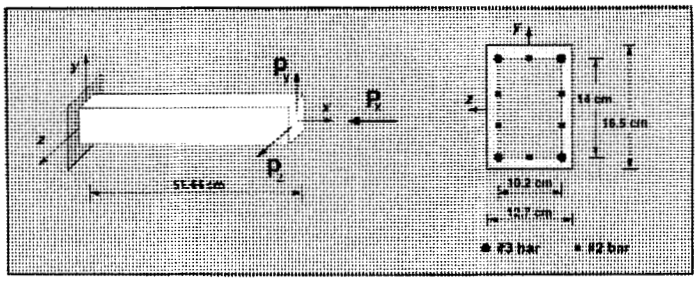

Figure 9. Geometry of specimens of Low and Moehle[10]

Table VI. Discretization of column Specimen #1 and #2 of Low–Moehle

Low–Moehle Specimens #1 and #2				
Number of beam–column elements: 1				
Length of element = 20·25 in		Number of Sections = 4		
	Number of fibres			
Section type	Unconfined concrete	Confined concrete	Steel	Total
I and II	4×8 + 15×4	16×12	10	294

Table VII. Concrete and steel material properties (1 ksi = 6·894 MPa)

Concrete Properties				
Concrete type	E_c (ksi)	f'_c (ksi)	ε_0	ε_u
Unconfined (Sections I and II)	3700	−5·30	−0·00200	−0·0119
High Confinement (Section I)	3700	−6·53	−0·00246	−0·3710
Medium Confinement (Section II)	3700	−6·11	−0·00231	−0·2330

Steel Properties			
Steel type	E_s (ksi)	f_y (ksi)	Strain hardening ratio
Steel type 1	29,000	64·9	0·0067
Steel type 2	29,000	64·4	0·0038
Steel type 3	29,000	73·1	0·0050

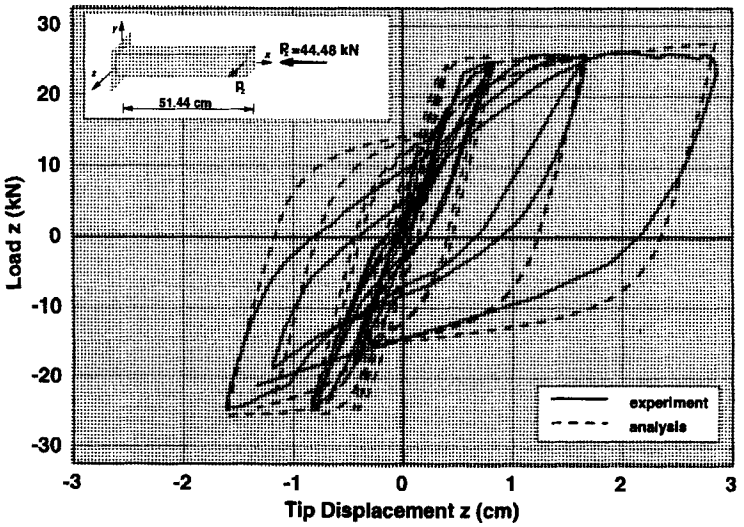

Figure 10. Comparison of analytical with experimental results for tip load–displacement relation in the z-direction of Low–Moehle specimen #1: uniaxial bending with axial load

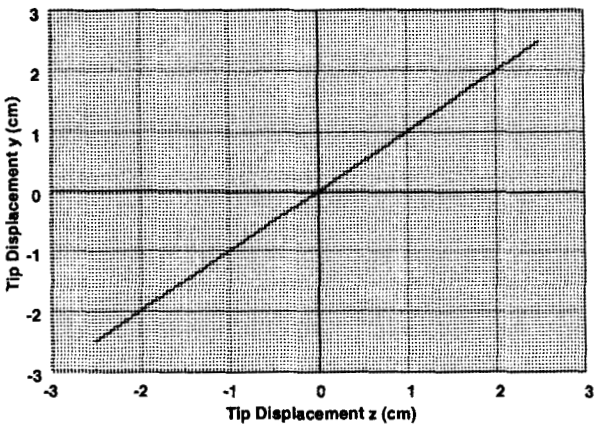

(a)

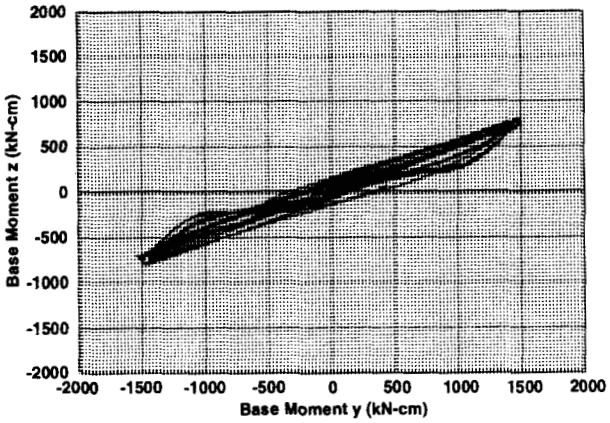

(b)

Figure 11. Load history for model of Low–Moehle Specimen #2: (a) imposed tip displacements; (b) base moment response

The analytical results are compared with the measured tip load–displacement relation in Figure 10. The agreement between experimental and analytical results is good even though the model is clearly stiffer than the specimen, particularly, in the early stages of the hysteretic response. The stiffness discrepancy at the very early stage of the response can be attributed to the initial cracking of the specimen due to shrinkage and temperature. The discrepancy in hysteretic behaviour under large displacement reversals, on the other hand, can be attributed to the significant effect of bond-slip and pull-out of the longitudinal reinforcing bars from the foundation. Since the numerical simulations are conducted under displacement control this effect is only evident in the 'pinching' of the hysteretic response and the earlier loss of strength of the specimen relative to the model.

Specimen #2 was subjected to a cyclic lateral force at the free end of the cantilever so as to induce lateral displacements at 45° relative to the principal axes of the specimen, while the axial load was maintained equal to a compression value of 44·5 kN throughout the test. The imposed cyclic displacement history is shown in Figure 11(a), while Figure 11(b) shows the resulting bending moment history at the base of the column. The moment ratio does not coincide with the imposed displacement ratio, so that a small hysteretic loop results. The experimental and analytical tip load–displacement relations relative to the principal axes of the cross-section are shown in Figures 12 and 13. The agreement is very good, with the common discrepancy in the 'pinching' of the hysteretic response, as a result of the absence of bond-slip and shear deformations from the

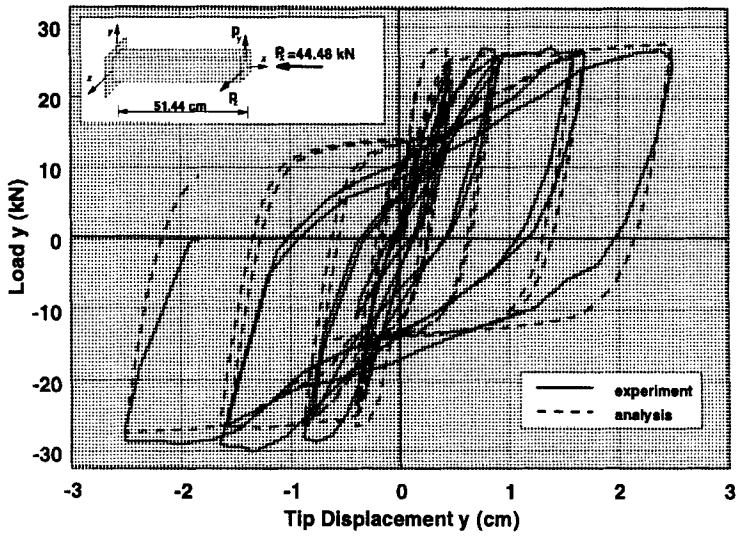

Figure 12. Comparison of analytical with experimental results for tip load–displacement relation in the y-direction of Low–Moehle Specimen #2: biaxial bending with axial load

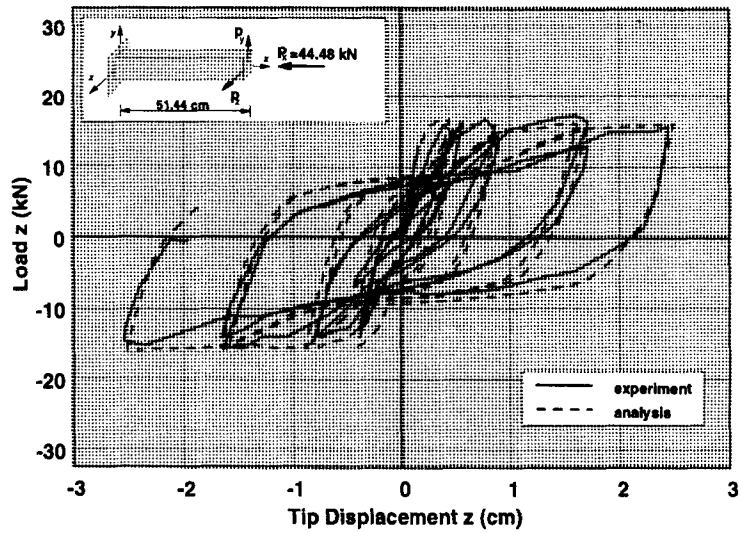

Figure 13. Comparison of analytical with experimental results for tip load–displacement relation in the z-direction of Low–Moehle Specimen #2: biaxial bending with axial load

analytical model. The fixed-end rotation due to pull-out of the reinforcement from the base of the column is rather small and accounts for only 5 per cent of the tip displacement. The model is clearly stiffer than the specimen in the early stages of the hysteretic response when the initial cracking state of the specimen as a result of shrinkage and temperature effects cannot be readily simulated. The cyclic strain history in the four corner reinforcing bars is shown in Figure 14.

The dramatic effect of a high axial compression load on the hysteretic response of Specimen #2 can be seen in Figures 15 and 16. For the same lateral displacement history as in Figure 11, but with an axial force of 334 kN that corresponds to approximately 35 per cent $f'_c A_c$, and varies between the values of 200 kN ($\sim$20 per cent $f'_c A_c$) and 467 kN ($\sim$50 per cent $f'_c A_c$) in proportion to the imposed lateral displacement, the column

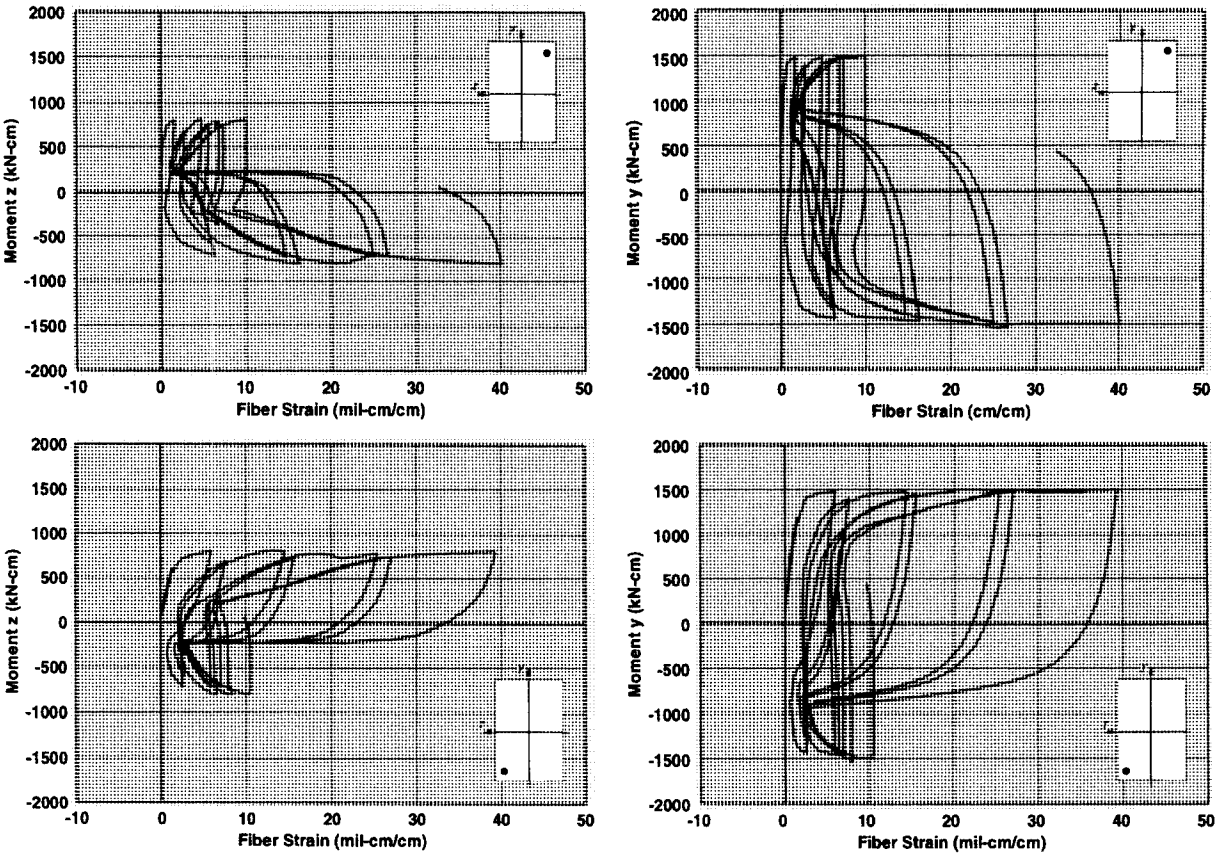

Figure 14. Strain history for corner reinforcing bars of Low–Moehle Specimen #2

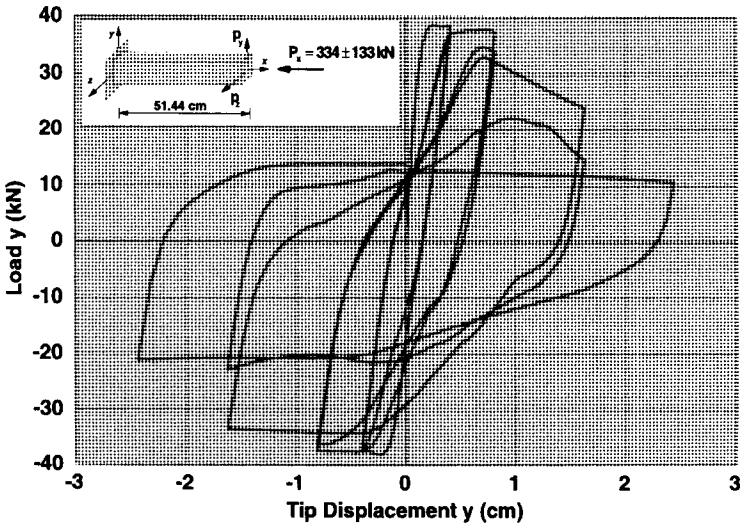

Figure 15. Simulation of hysteretic behaviour of Low–Moehle Specimen #2 under cyclic axial and biaxial lateral force: tip load–displacement relation in y-direction

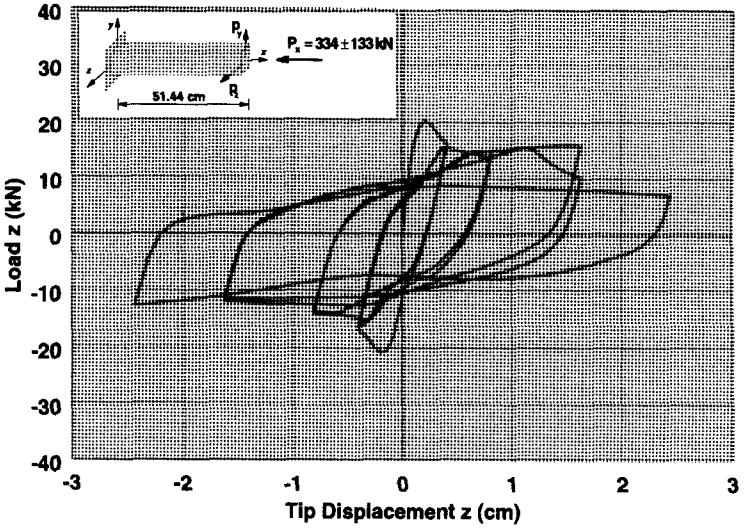

Figure 16. Simulation of hysteretic behaviour of Low–Moehle Specimen #2 under cyclic axial and biaxial lateral force: tip load–displacement relation in z-direction

is not able to maintain its lateral load carrying capacity past a tip displacement of about 1 cm. This example also serves as a clear illustration of the capability of the proposed beam-column model to represent the hysteretic behaviour of reinforced concrete members under complex loading histories without numerical difficulties, even in the presence of significant strength loss.

BIAXIAL BENDING WITH VARIABLE AXIAL COMPRESSION

Specimen #5 in the test series of Low and Moehle was subjected to a rather complex load history of biaxial bending with variable axial force intended to simulate loading conditions in structures under bidirectional acceleration input and torsional effects. The imposed tip displacement history is shown in Figure 17(a) and the variation of axial force in Figure 17(b). The resulting history of the column base moments is shown in Figure 18. The accumulation of damage and the variation of axial force causes a strong deviation of the moment relation from the imposed tip displacement history in Figure 17(a). The agreement between experimental and analytical results in Figures 19 and 20 is very satisfactory, even though the discrepancy in the 'pinching' behaviour of the load–displacement relation is again noticeable. It can, thus, be concluded that the effects of shear and bond-slip of longitudinal reinforcing steel play a significant role in the reloading phase of the hysteretic response, in spite of their small contribution to the maximum tip displacement of the cantilever column. Finally, Figure 21 depicts the complex strain history that two corner reinforcing bars of Specimen #5 experience.

CONCLUSIONS

This paper presents correlation studies of the fibre beam-column model that is proposed in the companion paper by Spacone *et al.*[1] with experimental results. The selected specimens are of gradually increasing complexity starting from a reinforced concrete section, followed by a cantilever beam with no axial force and concluding with a cantilever column under constant as well as varying axial force. While the section and cantilever beam are subjected to a cyclic uniaxial curvature and a cyclic uniaxial tip displacement, respectively, the cantilever column is investigated under three different load histories: a uniaxial cyclic tip displacement in one principal direction; a cyclic tip displacement in a direction that does not coincide with a principal axis and, thus, induces biaxial response; and, a cyclic tip displacement in a cloverleaf pattern with simultaneously varying axial force.

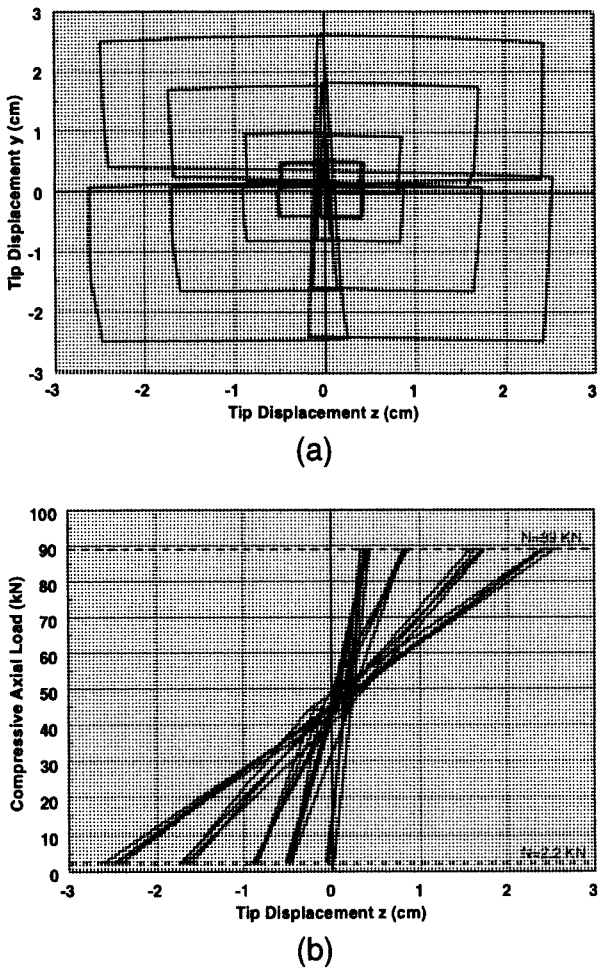

Figure 17. Load history for model of Low–Moehle Specimen #5: (a) imposed tip displacements; (b) applied axial load

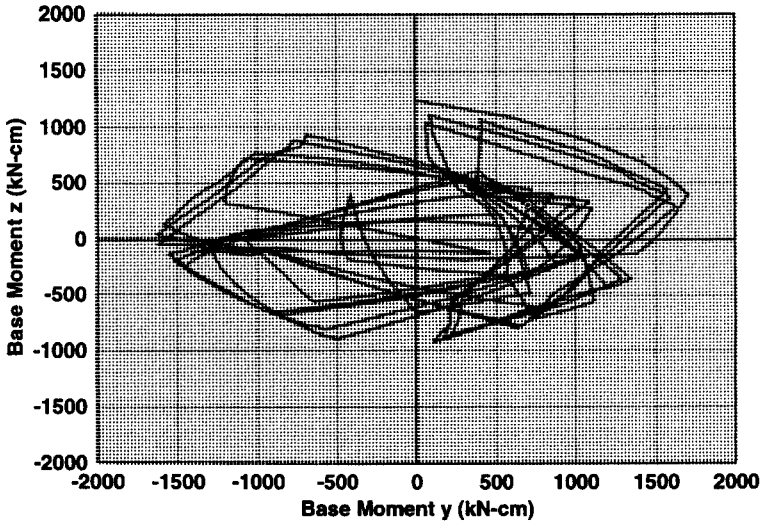

Figure 18. Base moment response for Low–Moehle Specimen #5

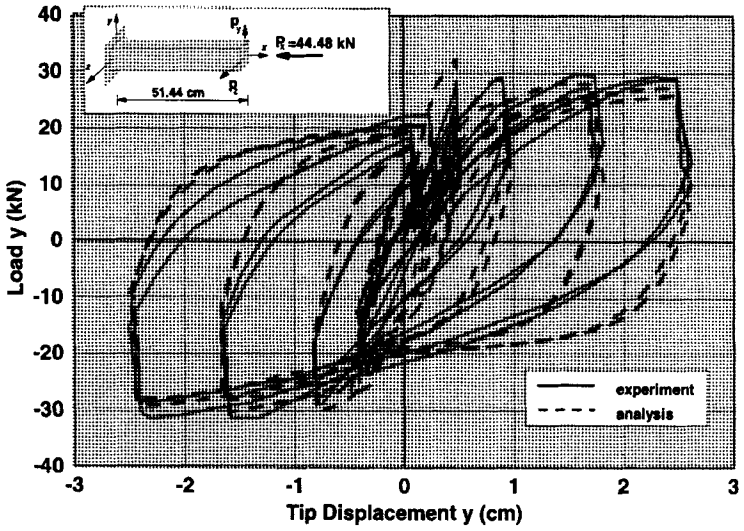

Figure 19. Comparison of analytical with experimental results for tip load–displacement relation in the y-direction of Low–Moehle Specimen #5: biaxial bending with cyclic axial load

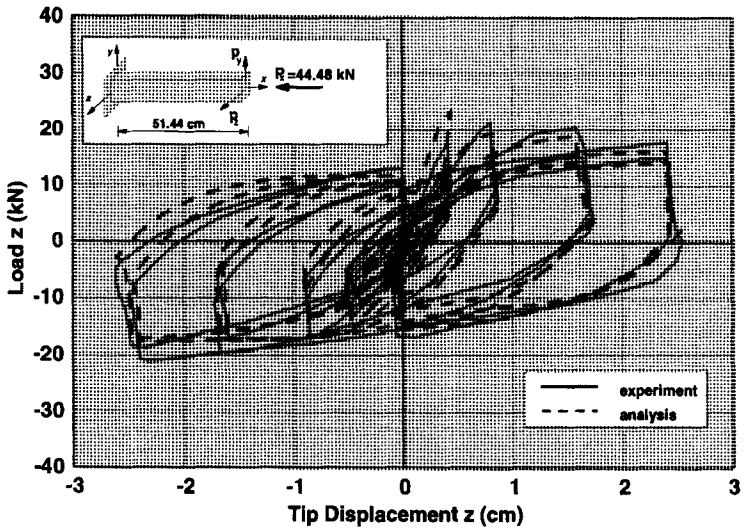

Figure 20. Comparison of analytical with experimental results for tip load–displacement relation in the z-direction of Low–Moehle Specimen #5: biaxial bending with cyclic axial load

The results of the proposed fibre model show very good agreement with data from pseudo-static experiments, especially, for cycles that induce small to average damage in the members under investigation. Since the proposed beam-column element does not account for shear deformations, the specimen selection for testing the validity of the model is limited to cases with small shear contribution to member deformations. Under very large inelastic deformations the fibre model yields higher resisting forces than those measured in experiments. This can be expected on account of the fact that the material models of the constituent fibres do not include the effect of cyclic damage of unconfined and confined concrete, the buckling of the longitudinal reinforcing bars and the effect of shear and bond-slip of reinforcing bars on the damage state of the member. These refinements can be readily added to the fibre material models in future studies. Moreover, the model

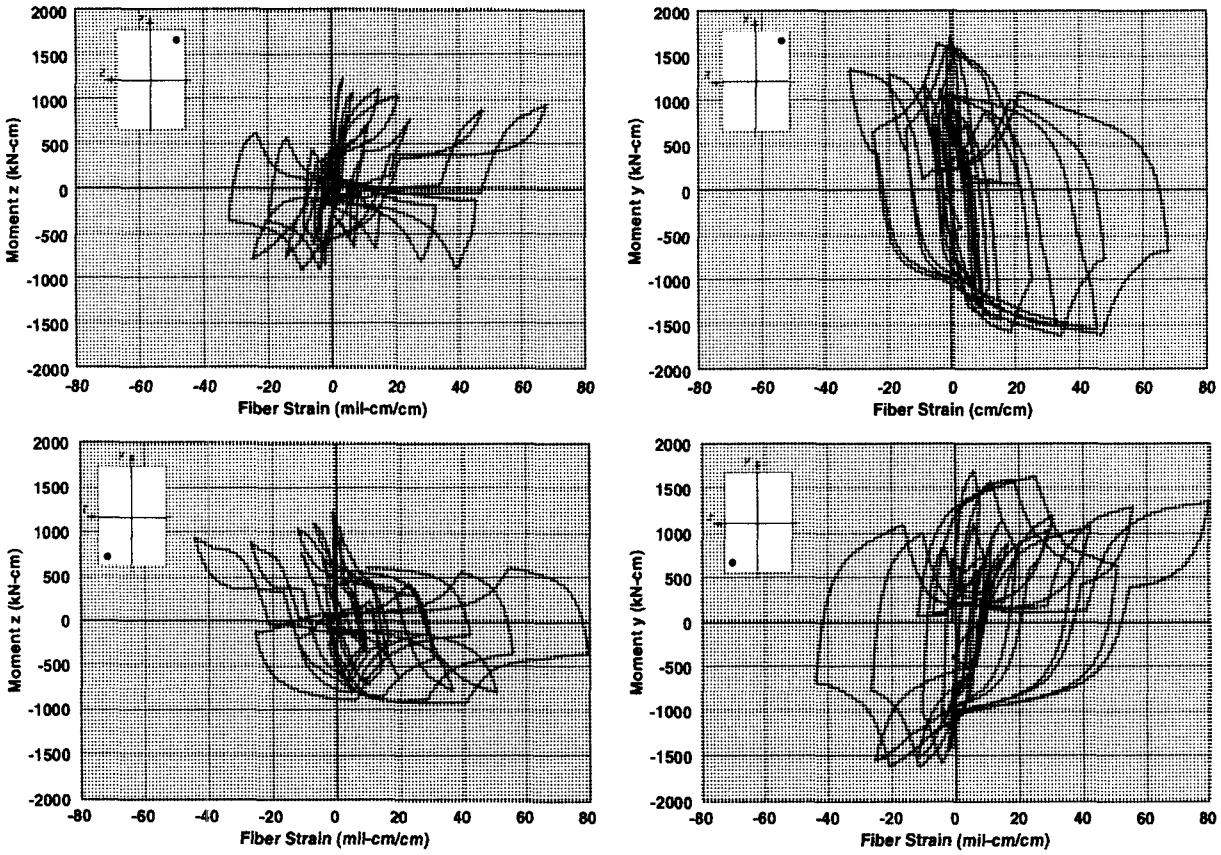

Figure 21. Strain history for corner reinforcing bars of Low–Moehle Specimen #5

does not account for the fixed end rotation due to reinforcing bar pull-out from the base of the specimen. Under imposed displacement conditions the bar pull-out has a slight effect on the load carrying capacity of the specimen, but it affects significantly the reloading stiffness and energy dissipation capacity.

The advantages of the proposed element over classical stiffness-based models are: (a) the robust numerical behaviour, that is demonstrated through stable convergence characteristics even in the presence of softening and strength loss, and, (b) the ease of inclusion of distributed element loads in the flexibility-based element. The latter is a very useful feature for the non-linear analysis of prestressed concrete members, as demonstrated by Mohd Yassin[11] and for the modelling of distributed bond in anchored reinforcing bars, as demonstrated by Monti *et al.*[12] Even though the proposed element state determination is more time consuming from a computational standpoint than that of a stiffness based element, the overall computational cost of the non-linear analysis is smaller on account of the smaller number of elements in the structural model and the reduction in the number of Newton–Raphson iterations at the global degrees of freedom due to the numerical stability of the state determination process. The quantitative assessment of the latter aspect will be addressed in a future paper.

ACKNOWLEDGMENTS

This work is part of a larger study on the non-linear analysis of reinforced concrete buildings under earthquake excitations sponsored by Grant ECE-8657525 from the National Science Foundation. This support is gratefully acknowledged. Any opinions expressed in this report are those of the authors and do not reflect the views of the sponsoring agency.

The authors would like to thank Professor R. L. Taylor of the University of California, Berkeley for his tireless assistance with the intricacies of program FEAP and Professor V. Ciampi of the University of Rome, La Sapienza for fruitful discussions during the course of this study.

APPENDIX. NOTATION

The following symbols are used in this paper:

A_c	concrete area
E_c	initial concrete modulus
E_s	initial steel modulus
f'_c	concrete compressive strength
f_y	yield strength of reinforcing steel
ε_0	strain at concrete compressive strength
ε_u	ultimate concrete strain

REFERENCES

1. E. Spacone, F. C. Filippou and F. F. Taucer, 'Fiber beam-column model for non-linear analysis of RC frames: Part I. formulation', *Earthquake eng. struct. dyn.* **25**, 711–725 (1996).
2. F. C. Filippou, 'FEDEAS—Finite elements for design, evaluation, and analysis of structures—reference manual and examples', *SEMM Report 96/XX*, Department of Civil Engineering, University of California, Berkeley, 1996, to appear.
3. O. C. Zienkiewicz and R. L. Taylor, *The Finite Element Method. Vol. 1. Basic Formulation and Linear Problems*, 4th edn., McGraw-Hill, London, 1989.
4. O. C. Zienkiewicz and R. L. Taylor, *The Finite Element Method. Vol. 2. Solid and Fluid Mechanics, Dynamics and Non-Linearity*, 4th edn., McGraw-Hill, London, 1991.
5. E. Spacone, 'Flexibility-based finite element models for the nonlinear static and dynamic analysis of concrete frame structures', *Ph.D. Dissertation*, Department of Civil Engineering, University of California, Berkeley, 1994.
6. D. C. Kent, 'Inelastic behavior of reinforced concrete members with cyclic loading', *Ph.D. Dissertation*, University of Canterbury, Christchurch, New Zealand, 1969.
7. B. D. Scott, R. Park and M. J. N. Priestley, 'Stress–strain behavior of concrete confined by overlapping hoops at low and high strain rates', *ACI j.* **79**, 13–27 (1982).
8. F. F. Taucer, E. Spacone and F. C. Filippou, 'A fiber beam-column element for seismic response analysis of reinforced concrete structures', *EERC Report 91/17*, Earthquake Engineering Research Center, University of California, Berkeley, 1991.
9. S. Y. Ma, V. V. Bertero and E. P. Popov, 'Experimental and analytical studies on the hysteretic behavior of reinforced concrete rectangular and T-beams', *EERC Report 76/02*, Earthquake Engineering Research Center, University of California, Berkeley, 1976.
10. S. S. Low and J. P. Moehle, 'Experimental study of reinforced concrete columns subjected to multi-axial cyclic loading', *EERC Report 87/14*, Earthquake Engineering Research Center, University of California, Berkeley, 1987.
11. M. Y. Mohd Yassin, 'Nonlinear analysis of prestressed concrete structures under monotonic and cyclic loads', *Ph.D. Dissertation*, Department of Civil Engineering, University of California, Berkeley, 1994.
12. G. Monti, E. Spacon, and F. C. Filippou, 'Model for anchored reinforcing bars under cyclic excitations', *EERC Report 93/08*, Earthquake Engineering Research Center, University of California, Berkeley, 1993.
13. S. Kaba and S. A. Mahin, 'Refined modeling of reinforced concrete columns for seismic analysis', *EERC Report 84/03*, Earthquake Engineering Research Center, University of California, Berkeley, 1984.